# Pathway of ATP Hydrolysis by Monomeric Kinesin Eg5†

Jared C. Cochran,‡ Troy C. Krzysiak, and Susan P. Gilbert*

*Department of Biological Sciences, University of Pittsburgh, Pittsburgh, Pennsylvania 15260*

*Received May 1, 2006; Revised Manuscript Received July 7, 2006*

ABSTRACT: Kinesin-5 family members including human Eg5/KSP contribute to the plus-end-directed force necessary for the assembly and maintenance of the bipolar mitotic spindle. We have used monomeric Eg5-367 in the nucleotide-free state to evaluate the role of microtubules at each step in the ATPase cycle. The pre-steady-state kinetic results show that the microtubule−Eg5 complex binds MgATP tightly, followed by rapid ATP hydrolysis with a subsequent slow step that limits steady-state turnover. We show that microtubules accelerate the kinetics of each step in the ATPase pathway, suggesting that microtubules amplify the nucleotide-dependent structural transitions required for force generation. The experimentally determined rate constants for phosphate product release and Eg5 detachment from the microtubule were similar, suggesting that these two steps are coupled with one occurring at the slow rate after ATP hydrolysis followed by the second step occurring more rapidly. The rate of this slow step correlates well with the steady-state $k_{cat}$, indicative that it is the rate-limiting step of the mechanism.

Kinesins are cytoskeletal motor proteins that utilize the energy from the ATPase cycle to perform mechanical work along microtubules. Conversion of the nucleotide state at the motor active site triggers conformational changes in the motor, which dictates the affinity of the motor for its filament and ultimately results in force generation. Although the specific structural events linking the ATP hydrolysis cycle to molecular motion are unknown, a mechanism for the pathway of conformational change that is responsible for amplifying small movements at the nucleotide binding site to large-scale changes in distant regions of the motor is now emerging.

Kinesins share an ∼350 amino acid motor domain that contains the nucleotide binding site and the microtubule binding region (reviewed in refs *1* and *2* and also see the kinesin homepage: http://www.proweb.org/kinesin/). A third region that is conserved within kinesin subfamilies is the ∼14−20 amino acid sequence adjacent to the motor domain called the neck linker. Together, the motor domain and the neck linker make up the core domain, and numerous studies have investigated the ATPase mechanism of different kinesin monomers in the presence of microtubules including Kinesin-1/conventional kinesin (*3*−*8*), Kinesin-5/Eg5/BimC (*9*−*11*), and Kinesin-14/Ncd/Kar3/ (*12*−*15*). The structural differences that arise between various kinesin subfamilies have fine-tuned the rate and equilibrium constants that govern the overall mechanochemical cycles. Therefore, each kinesin motor elicits a different work output that is utilized to perform different tasks, including vesicle transport, regulation of microtubule dynamics, and mitotic spindle assembly and chromosome segregation.

Kinesin-5 family members share a similar homotetrameric quaternary structure with two dimers positioned at each end of a coiled-coil stalk (*16*−*18*). This bipolar structure facilitates the ability of Kinesin-5 to interact with and slide adjacent microtubules during mitosis, thus contributing to the plus-end-directed force that is necessary to form and maintain the mitotic spindle (*19*−*30*). Due to the importance of Kinesin-5 for mitosis, several studies have identified Kinesin-5 inhibitors (*31*−*40*) that can be used in the treatment of cancer and other diseases of abnormal mitotic index (reviewed in refs *41* and *42*).

Previous studies have focused on characterizing the fundamental kinetic mechanism of monomeric human Eg5 (KSP/Kinesin-5) in the absence (*43*) and presence of microtubules (*9*, *10*). These studies have revealed a mechanochemical cycle for Mt·Eg5[1] that is similar to conventional Kinesin-1 based on rapid microtubule association kinetics, fast ADP product release, two-step ATP binding, relatively fast ATP hydrolysis, and a rate-limiting slow step after ATP hydrolysis. These kinetic steps are intimately related to the changes in Eg5's neck-linker orientation for force generation and processive stepping (*10*, *44*, *45*). Previous analyses from our laboratory of the Eg5 ATPase mechanism were performed with two monomeric, truncated Eg5 proteins (Eg5-367 and Eg5-437). However, several important steps in the

† This work was supported by NIH Grant GM54141 from NIGMS and NIH K02-AR47841 Career Development Award from NIAMS to S.P.G.

* Corresponding author. Tel: 412-624-5842. Fax: 412-624-4759. E-mail: spg1@pitt.edu.

‡ Present address: Department of Chemistry, Dartmouth College, Hanover, NH 03755.

[1] Abbreviations: Eg5-367, human Eg5/KSP motor domain containing the N-terminal 367 residues followed by a C-terminal $His_6$ tag; Eg5-437, human Eg5/KSP motor domain containing the N-terminal 437 residues followed by a C-terminal $His_6$ tag; apoEg5, nucleotide-free Eg5-367; MDCC-PBP, 7-(diethylamino)-3-[[[(2-maleimidyl)ethyl]amino]carbonyl]coumarin-labeled phosphate binding protein; PNPase, purine nucleotide phosphorylase; MEG, 7-methylguanosine; $P_i$, inorganic phosphate; Mt, microtubule; mant, 2′(3′)-*O*-(*N*-methylanthraniloyl); AMPPNP, adenosine 5′-($\beta$,$\gamma$-imino)triphosphate.

10.1021/bi0608562 CCC: $33.50 
Published on Web 09/15/2006

Eg5 ATPase mechanism have not been characterized. In addition, we have recently defined the ATPase cycle of Eg5 in the absence of microtubules using apoEg5 which is nucleotide-free (*43*). We can now make a direct comparison at each step of the ATPase cycle in the presence and absence of microtubules to understand the structural transitions that establish the bipolar mitotic spindle.

In the present study, we investigated the microtubule-activated ATPase mechanism of apoEg5-367. We have characterized the activity of apoEg5 preparations by steady-state ATPase kinetics as well as investigated the pre-steady-state kinetics of microtubule association, MgATP binding, ATP hydrolysis, inorganic phosphate ($P_i$) product release, and motor detachment from the microtubule. We show that microtubules activate the rate of every step in the ATPase pathway rather than just accelerating the rate of a single step. In addition, we propose that the kinetic steps of $P_i$ product release and Eg5 detachment from the microtubule are coupled, and the observed rate of either step when measured experimentally correlates well with the steady-state $k_{cat}$. These results indicate that the overall kinetic mechanism of monomeric Eg5 can satisfy the demands of having the motor tightly bound to the microtubule during a majority of its ATPase cycle to generate and sustain force in the mitotic spindle.

## MATERIALS AND METHODS

*Experimental Conditions.* Experiments reported here were performed at 25 °C in ATPase buffer (20 mM Hepes, pH 7.2, with KOH, 5 mM magnesium acetate, 0.1 mM EDTA, 0.1 mM EGTA, 50 mM potassium acetate, 1 mM dithiothreitol, 5% sucrose) with the concentrations reported as final after mixing.

*Protein Preparation.* In this study we have expressed and purified nucleotide-free human Eg5-367 (apoEg5) as described previously (*9*, *43*, *46*). Briefly, magnesium chloride and ATP were excluded from all column chromatography buffers. The enriched Eg5 fractions from the nickel nitrilotriacetic acid−agarose column (Qiagen, Valencia, CA) were pooled and incubated with 5 mM EGTA and 5 mM EDTA. The mixture was loaded onto a Bio-Gel P-6 size exclusion column (Bio-Rad Laboratories Inc.) to remove chelating reagents and any residual nucleotide. The elution volume containing the excluded apoEg5 was concentrated by ultrafiltration and dialyzed against ATPase buffer. We determined the apoEg5 protein concentration by the Bio-Rad protein assay with IgG as the standard. The nucleotide-free determination of our apoEg5 preparations was performed as described previously (*43*). On the day of each experiment, an aliquot of purified bovine brain tubulin was thawed and cycled, and the microtubules were stabilized with 20 $\mu$M Taxol (paclitaxel; Sigma-Aldrich Co.).

*Steady-State ATPase.* The ATPase activity of apoEg5 was determined by following [$\alpha$-$^{32}$P]ATP hydrolysis to form [$\alpha$-$^{32}$P]ADP·$P_i$ as previously described (*47*). Briefly, the steady-state ATPase kinetics of apoEg5 were measured as a function of MgATP concentration at saturating microtubule concentration and as a function of microtubule concentration at saturating MgATP. For the ATP concentration dependence experiments (Figure 1), the rate of ATP turnover was plotted as a function of MgATP concentration, and the data were fit to the Michaelis−Menten equation. For the microtubule concentration dependence experiments (Figure 1, inset), the rate of ATP turnover was plotted against tubulin concentration, and the data were fit to the quadratic equation:

$$\text{rate} = 0.5k_{cat}\{(E_0 + K_{1/2,Mt} + [Mt]) - [(E_0 + K_{1/2,Mt} + [Mt])^2 - (4E_0[Mt])]^{1/2}\} \quad (1)$$

where $E_0$ is the Eg5 site concentration, $K_{1/2,Mt}$ is the tubulin concentration as microtubules needed to provide one-half of the maximal velocity, and [Mt] is the tubulin concentration as microtubule polymer.

*Mt·Eg5 Cosedimentation Assays in the Absence of Nucleotide.* Cosedimentation experiments were performed as described (*9*, *48*) where apoEg5 and Eg5·ADP (1 mol of apoEg5 plus 1 mol of MgADP) were incubated with microtubules for 30 min, and the Mt·Eg5 complexes were pelleted by centrifugation in a Beckman Airfuge (Beckman Coulter Inc., Fullerton, CA) at 30 psi (100000*g*) for 30 min. Gel samples were prepared for the supernatant and pellet fractions at equal volumes for each reaction, and the proteins were resolved by SDS−PAGE and stained with Coomassie brilliant blue R-250 (Figure 2, inset).

*Rapid Chemical Quench-Flow Experiments.* The pre-steady-state kinetics of MgATP binding and ATP hydrolysis were determined by utilizing pulse−chase and acid−quench methodologies, respectively, using a KinTek RQF-3 chemical quench-flow instrument (KinTek Corp., Austin, TX) (*9*). In the pulse−chase experiments, a preformed Mt·Eg5 complex was rapidly mixed with increasing [$\alpha$-$^{32}$P]MgATP concentrations plus KCl, and the reaction was continued for various times (5−500 ms) followed by the nonradioactive MgATP chase (30 mM in syringe, 10 mM final) for 3 s (~10 turnovers). The additional KCl was added to the [$\alpha$-$^{32}$P]ATP syringe to lower Eg5 steady-state ATPase activity without affecting the kinetics of ATP binding or ATP hydrolysis during the first turnover. The concentration of [$\alpha$-$^{32}$P]ADP product was plotted as function of time, and each pulse−chase transient was fit to the burst equation (Figure 3A):

$$\text{product} = A_0[1 - \exp(-k_b t)] + k_{ss}t \quad (2)$$

where $A_0$ corresponds to the concentration of tightly bound Mt·Eg5*·ATP complexes that proceed in the forward direction toward ATP hydrolysis for the pulse−chase experiments, $k_b$ is the rate constant of the exponential phase, and $k_{ss}$ is the rate constant of the linear phase ($\mu$M ADP·s$^{-1}$) corresponding to subsequent ATP turnovers.

In the acid−quench experiments, a preformed Mt·Eg5 complex was rapidly mixed with increasing [$\alpha$-$^{32}$P]MgATP concentrations plus KCl, and the reaction was continued for various times (0.005−1 s) followed by quenching with formic acid (5 M in syringe, 1.7 M final). The concentration of [$\alpha$-$^{32}$P]ADP product was plotted as function of time, and each acid−quench transient was fit to eq 2 (Figure 4A). For eq 2, $A_0$ corresponds to the concentration of [$\alpha$-$^{32}$P]ADP·$P_i$ product formed at the active site during the first ATP turnover, and $k_b$ is the rate constant of exponential product formation at the active site during the first ATP turnover. For both pulse−chase (Figure 3B) and acid−quench experiments (Figure 4B), the amplitude and rate of the exponential

Scheme 1

$$\mathrm{M{\cdot}E + ATP} \underset{k_{-1}}{\overset{k_{+1}}{\rightleftharpoons}} \mathrm{M{\cdot}E{\cdot}ATP} \underset{k_{-1'}}{\overset{k_{+1'}}{\rightleftharpoons}} \mathrm{M{\cdot}E^{*}{\cdot}ATP} \underset{k_{-2}}{\overset{k_{+2}}{\rightleftharpoons}} \mathrm{M{\cdot}E{\cdot}ADP{\cdot}P_i} \underset{k_{-3}}{\overset{k_{+3}}{\rightleftharpoons}} \mathrm{M + E{\cdot}ADP + P_i} \underset{k_{-4}}{\overset{k_{+4}}{\rightleftharpoons}} \mathrm{M{\cdot}E + ADP}$$

burst phase for each transient were plotted against MgATP concentration, and each data set was fit to a hyperbola.

*Data Analysis.* The kinetics of ATP binding and hydrolysis were analyzed by a four-step model using KINSIM (*49*):

$$\mathrm{M{\cdot}E + ATP} \overset{k_{+1}}{\rightleftharpoons} \mathrm{M{\cdot}E{\cdot}ATP} \overset{k_{+1'}}{\rightleftharpoons} \mathrm{M{\cdot}E^{*}{\cdot}ATP} \overset{k_{+2}}{\rightleftharpoons} \mathrm{M{\cdot}E{\cdot}ADP{\cdot}P_i} \overset{k_{slow}}{\rightleftharpoons} \mathrm{M + E{\cdot}ADP + P_i} \quad (3)$$

where M·E represents the microtubule−apoEg5 complex with 5 $\mu$M apoEg5, $k_{+1}$ is the apparent second-order rate constant for ATP binding, $k_{+1'}$ is the rate constant for the ATP-promoted conformational change that occurs prior to ATP hydrolysis, $k_{+2}$ denotes the rate constant for ATP hydrolysis, and $k_{slow}$ is the rate of the slow step in the pathway that occurs after ATP hydrolysis. The intrinsic rate constants determined from the KINSIM analysis and provided in Table 2 fit the data at three ATP concentrations (Figure 4C) and satisfied the equations

$$k_{cat} = k_{+2}k_{slow}/(k_{+2} + k_{-2} + k_{slow}) \quad (4)$$

and

$$A_0 = E_0[k_{+2}(k_{+2} + k_{-2})/(k_{+2} + k_{-2} + k_{slow})^2] \quad (5)$$

where $k_{cat}$ is the turnover number based on steady-state ATPase and $A_0$ is the amplitude of the pre-steady-state burst phase of the ATP hydrolysis time dependence that corresponds to the accumulation of product at the Eg5 active site during the first ATP turnover.

*Stopped-Flow Experiments.* The SF-2003 KinTek stopped-flow instrument (KinTek Corp.) was used to measure the kinetics of Eg5 association with microtubules (Figure 2), $P_i$ product release from the Mt·Eg5 complex (Figure 5), and ATP-promoted Eg5 detachment from the microtubule (Figure 6). $P_i$ product release from the Mt·Eg5 complex was determined using the MDCC-PBP coupled assay, as described previously (*43*, *50*−*52*). A preformed Mt·Eg5 complex plus MDCC-PBP and "$P_i$ mop" were rapidly mixed with increasing MgATP concentrations plus KCl and $P_i$ mop. The $P_i$ mop removes the 1−2 $\mu$M contaminating $P_i$ that is present in the buffers, and the concentrations of "Mop" reagents (PNPase, MEG) were experimentally determined to eliminate competition with the MDCC-PBP for $P_i$ during the reaction. The experimental design assumes that, after ATP hydrolysis, $P_i$ product will be released from the active site of Eg5 and bind rapidly and tightly to MDCC-PBP, thus triggering the fluorescence enhancement of the MDCC-PBP·$P_i$ complex (*51*). In order to convert the observed change in fluorescence intensity into units of $P_i$ concentration, a phosphate standard curve was used (data not shown).

The kinetics of apoEg5 association with microtubules (Figure 2) and ATP-promoted dissociation of the Mt·Eg5 complex (Figure 6) were determined by monitoring the change in solution turbidity at 340 nm. In Figure 2, the observed exponential rate of motor association with microtubules was plotted as a function of microtubule concentration and fit to the equation:

$$k_{obs} = k_{+5}[\mathrm{tubulin}] + k_{-5} \quad (6)$$

where $k_{obs}$ is the rate constant of the exponential phase, $k_{+5}$ is the apparent second-order rate constant for Eg5 association with microtubules (Scheme 1), and $k_{-5}$ corresponds to the observed rate constant for motor dissociation from the Mt·Eg5 complex as determined from the *y*-intercept. In Figure 6, the exponential rate of Mt·Eg5 dissociation was plotted as a function of MgATP concentration, and the data were fit to a hyperbola to determine the dissociation rate constant $k_{+3}$ (Scheme 1).

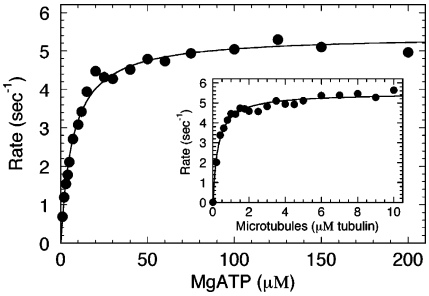


FIGURE 1: Microtubule-activated steady-state ATPase of apoEg5. The Mt·Eg5 complex was preformed with Taxol-stabilized microtubules, and the reaction was initiated by mixing with varying concentrations of MgATP. Final concentrations: 70 nM apoEg5, 10 $\mu$M tubulin, 30 $\mu$M Taxol, and 1−200 $\mu$M [$\alpha$-$^{32}$P]MgATP. The data were fit to the Michaelis−Menten equation: $k_{cat} = 5.4 \pm 0.1$ s$^{-1}$ and $K_{m,ATP} = 7.0 \pm 0.4$ $\mu$M. Inset: Microtubule concentration dependence. Final concentrations: 75 nM apoEg5, 0−10 $\mu$M tubulin, 20 $\mu$M Taxol, and 500 $\mu$M [$\alpha$-$^{32}$P]MgATP. The data were fit to eq 1: $k_{cat} = 5.5 \pm 0.1$ s$^{-1}$ and $K_{1/2,Mt} = 0.29 \pm 0.02$ $\mu$M.

## RESULTS

*ApoEg5 Displays Normal Microtubule-Activated Steady-State ATPase.* Historically, when kinesin motors were purified, there was a tightly bound ADP at the active site (*53*), and attempts to isolate homogeneous, fully active kinesin in the nucleotide-free state were compromised due to the instability of the catalytic core in the absence of nucleotide (*12*, *48*, *54*, *55*). In spite of this general observation for kinesin motors, the structure of monomeric Eg5 permits the purification of fully active, stable Eg5 motors in the nucleotide-free state as we described previously (*43*).

We have pursued a mechanistic analysis of monomeric Eg5-367 in distinct nucleotide states: Eg5-367 bound to MgADP (Eg5·ADP) (*9*, *56*) and Eg5-367 in a stable, nucleotide-free state (apoEg5) (*43*). Both purification strategies resulted in the final Eg5 preparation at >99% purity. To test the microtubule-dependent activation of apoEg5 ATPase, we measured the kinetics of ATP turnover under steady-state conditions (Figure 1). If a significant fraction of the apoEg5 protein were inactive after removing nucleotide, then we would detect a decreased steady-state $k_{cat}$. However, the maximum rate of ATP turnover by apoEg5

Table 1: Experimentally Determined Constants for ApoEg5 and Mt·Eg5 ATPase

| | constant | apoEg5[a] | Mt·Eg5 |
|---|---|---|---|
| mantATP binding | $k_{+1}$ ($\mu M^{-1}$ $s^{-1}$) | 0.08 ± 0.01 | 3.4 ± 0.3[b] |
| | $k_{-1}$ ($s^{-1}$) | 0.09 ± 0.02 | 16.3 ± 0.6[b] |
| | $k_{+1'}$ ($s^{-1}$) | 0.85 ± 0.10 | 21.2 ± 1.3[b] |
| | $K_{1/2,mATP}$ ($\mu$M) | 9.9 ± 2.6 | 4.4 ± 1.1[b] |
| ATP binding (pulse−chase) | $k_{b,max}$ ($s^{-1}$) | 1.7 ± 0.3 | 19.7 ± 1.1 |
| | $K_{d,ATP}$ ($\mu$M) | 8.3 ± 6.3 | 14.2 ± 4.1 |
| | $A_{0,max}$ (ADP/site) | 0.14 ± 0.01 | 0.75 ± 0.02 |
| ATP hydrolysis (acid−quench) | $k_{b,max}$ ($s^{-1}$) | 1.14 ± 0.05 | 10.2 ± 0.7 |
| | $K_{d,ATP}$ ($\mu$M) | 12.7 ± 2.0 | 20.0 ± 6.6 |
| | $A_{0,max}$ (ADP/site) | 0.09 ± 0.002 | 0.75 ± 0.02 |
| | % of sites | 13 | 100 |
| phosphate release (MDCC-PBP) | $k_{b,max}$ ($s^{-1}$) | 0.54 ± 0.01 | 6.0 ± 0.1 |
| | $K_{1/2,ATP}$ ($\mu$M) | 6.3 ± 0.3 | 3.7 ± 0.2 |
| | $A_{0,max}$ ($P_i$/site) | 0.10 ± 0.003 | 0.75 ± 0.01 |
| | % of sites | 19 | 100 |
| Mt·Eg5 dissociation (turbidity) | $k_{max}$ ($s^{-1}$) | NA | 7.7 ± 0.2 |
| | $K_{1/2,ATP}$ ($\mu$M) | NA | 4.2 ± 0.3 |
| ADP release | $k_{max}$ ($s^{-1}$) | 0.05 ± 0.001 | 43.3 ± 0.2[b] |
| | $K_{1/2,Mt}$ ($\mu$M) | | 2.5 ± 0.1[b] |
| Mt·Eg5 association (turbidity) | $k_{on}$ ($\mu M^{-1}$ $s^{-1}$) | NA | 17 ± 2.2 |
| steady-state ATPase | $k_{cat}$ ($s^{-1}$) | 0.02 ± 0.003 | 5.4 ± 0.1 |
| | $K_{m,ATP}$ ($\mu$M) | 0.17 ± 0.03 | 7.0 ± 0.4 |
| | $k_{cat}/K_{m,ATP}$ ($\mu M^{-1}$ $s^{-1}$) | 0.12 | 0.77 |
| | $K_{1/2,Mt}$ ($\mu$M) | NA | 0.29 ± 0.02 |
| | $k_{cat}/K_{1/2,Mt}$ ($\mu M^{-1}$ $s^{-1}$) | NA | 18.6 |

[a] Mechanistic analysis of apoEg5 in the absence of microtubules (*43*). [b] Mechanistic analysis of the mitotic kinesin Eg5 in the presence of microtubules (*9*). NA, not applicable.

($k_{cat}$ = 5.4 $s^{-1}$) was comparable to Eg5·ADP ($k_{cat}$ = 5.5 $s^{-1}$), which suggests the enzymatic activity of apoEg5 preparations was similar to previously characterized Eg5·ADP (*9*). In addition, the Eg5 proteins shared similar $K_{m,ATP}$ and $K_{1/2,Mt}$ parameters. $K_{m,ATP}$ for apoEg5 = 7.0 $\mu$M versus Eg5·ADP = 9.5 $\mu$M and $K_{1/2,Mt}$ for apoEg5 = 0.29 $\mu$M versus Eg5·ADP = 0.71 $\mu$M (ref *9*; Table 1). The observed differences result from variability of different protein preparations rather than enzymatic or mechanistic differences. Together, these results indicate that Eg5 behaves similarly regardless of the purification strategy and the entire population of Eg5 sites reports during steady-state ATP turnover.

*ApoEg5 Rapidly Associates with the Microtubule.* To investigate the kinetics of apoEg5 association with microtubules, we utilized a stopped-flow instrument to monitor changes in solution turbidity as the motor associates with the microtubule lattice. Because it is the Eg5·ADP intermediate that binds microtubules, we preformed this intermediate using equimolar apoEg5 + MgADP (*9*). The observed rate of microtubule association increased linearly with microtubule concentration providing an apparent second-order rate constant, $k_{+5}$ at 20 $\mu M^{-1}$ $s^{-1}$ (Figure 2). This rate constant is faster than we reported previously and varies somewhat with the protein preparation (11−23.7 $\mu M^{-1}$ $s^{-1}$; mean = 17 ± 2.2 $\mu M^{-1}$ $s^{-1}$, $n$ = 5). The steady-state $k_{cat}/K_{1/2,Mt}$ predicts the lower limit of the second-order rate constant for microtubule association at 18.6 $\mu M^{-1}$ $s^{-1}$ (Table 1); therefore, the microtubule association constant is consistent with microtubule-activated steady-state ATP turnover.

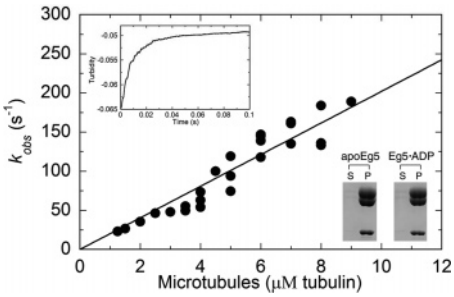


FIGURE 2: Microtubule−Eg5 interactions. The apoEg5·ADP intermediate was preformed and rapidly mixed in a stopped-flow instrument with increasing concentrations of microtubules. Final concentrations: 1.25 $\mu$M apoEg5, 1.25 $\mu$M MgADP for 1.25−2.5 $\mu$M tubulin, 2.5 $\mu$M apoEg5, 2.5 $\mu$M MgADP for 3−10 $\mu$M tubulin, and 20 $\mu$M Taxol. The observed rate obtained from the initial exponential phase of each transient was plotted as a function of microtubule concentration, and the data were fit to eq 6: $k_{on}$ = 20.2 ± 0.6 $\mu M^{-1}$ $s^{-1}$ (Scheme 1). Insets show a representative transient at 2.5 $\mu$M Eg5 and 5 $\mu$M tubulin polymer and a Coomassie blue-stained SDS−polyacrylamide gel from a Mt·Eg5 cosedimentation experiment using apoEg5 and Eg5·ADP (1:1). Final concentrations: 2 $\mu$M apoEg5, 0 or 2 $\mu$M MgADP, 4 $\mu$M tubulin, and 20 $\mu$M Taxol. After each reaction mixture was centrifuged, samples of the supernatant (S) and pellet (P) were loaded consecutively.

Mt·Eg5 cosedimentation assays were also performed to determine the microtubule binding behavior of the apoEg5 under equilibrium conditions. The inset of Figure 2 shows apoEg5 and Eg5·ADP partitioning with the microtubule pellet. These cosedimentation experiments were repeated at lower concentrations of the Mt·Eg5 complex (0.5 $\mu$M apoEg5, 1 $\mu$M tubulin), and similar results were obtained (data not shown). These results indicate that the apoEg5 motor is fully active and comparable to Eg5 purified with ADP at the active site. Therefore, we can make direct comparisons between the kinetics of apoEg5 in the absence of microtubules to the kinetics of the Mt·apoEg5 complex.

*The Entire Mt·Eg5 Population Binds MgATP Tightly during the First Turnover Event.* Previously, ATP binding to the Mt·Eg5-367 complex was investigated by mantATP fluorescence enhancement (*9*). These results suggested that ATP binding occurred in at least two steps: (1) rapid formation of the collision complex and (2) an isomerization event leading to a tightly ATP-bound state (Scheme 1). Using mantATP fluorescence enhancement, we were able to attain precise rate information, but we were not able to obtain amplitude information that provided the concentration of Eg5 sites that bound ATP and proceeded forward to ATP hydrolysis during the first turnover event.

To measure the pre-steady-state kinetics of [α-$^{32}$P]MgATP binding to the Mt·Eg5-367 complex, we performed pulse−chase experiments using a quench-flow instrument (Figure 3). The experimental design assumes any tightly bound [α-$^{32}$P]MgATP substrate will proceed in the forward reaction, while any loosely bound or unbound substrate will be diluted by the excess nonradioactive MgATP in the chase. Figure 3B shows that the rate of the exponential burst phase increased hyperbolically with [α-$^{32}$P]MgATP concentration, suggesting that an ATP-promoted isomerization of the Eg5 motor domain limits ATP binding. This structural transition forms the Mt·E*·ATP intermediate that proceeds directly to ATP hydrolysis (Scheme 1). The maximum observed rate ($k_{+1'}$) of the ATP-promoted conformational change was 19.7

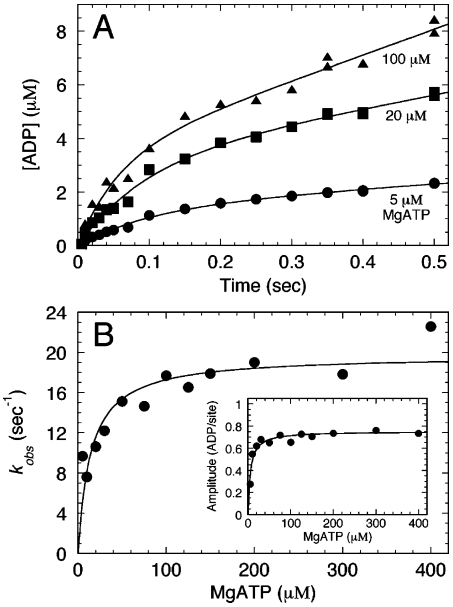


FIGURE 3: MgATP binding kinetics by pulse−chase. The Mt·Eg5 complex was reacted with increasing concentrations of [α-$^{32}$P]-MgATP for 5−500 ms in a quench-flow instrument, followed by the nonradioactive MgATP chase. Final concentrations: 5 $\mu$M apoEg5, 6 $\mu$M tubulin, 20 $\mu$M Taxol, 5−400 $\mu$M [α-$^{32}$P]MgATP, 100 mM KCl, and 10 mM nonradioactive MgATP chase. (A) Shown are time courses of [α-$^{32}$P]MgADP product formation (MgATP concentrations are indicated). Each transient displayed burst kinetics and was fit to eq 2 to provide the amplitude ($A_0$) and observed exponential rate ($k_b$) of the formation of a tightly ATP-bound Mt·Eg5*·ATP complex, followed by the linear phase corresponding to subsequent ATP turnovers ($k_{ss}$). (B) The exponential burst rates were plotted against MgATP concentration, and the data were fit to a hyperbola: $k_{b,max} = 19.7 \pm 1.1$ s$^{-1}$ with $K_{d,ATP} = 14.2 \pm 4.1$ $\mu$M. The inset shows the amplitude of the pre-steady-state burst phase versus MgATP concentration. $A_{0,max} = 0.75 \pm 0.02$ ADP/site with $K_{d,ATP} = 5.5 \pm 1.0$ $\mu$M.

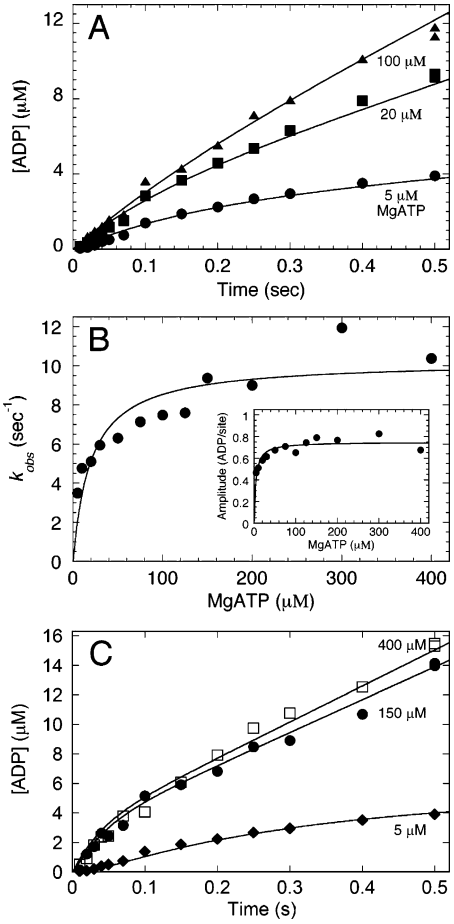


FIGURE 4: Kinetics of ATP hydrolysis by acid−quench. The Mt·Eg5 complex was reacted with increasing concentrations of [α-$^{32}$P]-MgATP plus KCl for 5−500 ms, followed by quenching with formic acid. Final concentrations: 5 $\mu$M apoEg5, 6 $\mu$M tubulin, 20 $\mu$M Taxol, 5−400 $\mu$M [α-$^{32}$P]MgATP, and 100 mM KCl. (A) Shown are representative time courses of [α-$^{32}$P]MgADP product formation (MgATP concentrations are indicated). Each transient displayed burst kinetics and was fit to eq 2 to provide the amplitude ($A_0$) and observed exponential rate ($k_b$) of the formation of the Mt·Eg5·ADP·P$_i$ intermediate, followed by the linear phase corresponding to subsequent ATP turnovers ($k_{ss}$). (B) The observed exponential rates were plotted against MgATP concentration, and the data were fit to a hyperbola: $k_{b,max} = 10.2 \pm 0.7$ s$^{-1}$ with $K_{d,ATP} = 20.0 \pm 6.6$ $\mu$M. The inset shows the amplitude of the exponential phase versus MgATP concentration. $A_{0,max} = 0.75 \pm 0.02$ ADP/site with $K_{d,ATP} = 4.2 \pm 1.0$ $\mu$M. (C) Data at 5, 150, and 400 $\mu$M MgATP were fit to the four-step model presented in Table 2 with the following intrinsic rate constants: $k_{+1} = 1$ $\mu$M$^{-1}$ s$^{-1}$, $k_{+1'} = 18$ s$^{-1}$, $k_{+2} = 20$ s$^{-1}$, $k_{slow} = 6.5$ s$^{-1}$ with $E_0 = 5$ $\mu$M apoEg5.

s$^{-1}$, similar to the observed rate for Eg5-367 determined by mantATP fluorescence enhancement at 21 s$^{-1}$ (*9*). The ATP binding kinetics reported here also correlate well with the kinetics of ATP-promoted neck-linker docking measured by fluorescence resonance energy transfer (FRET) experiments using a series of spectroscopic probes (*10*). Therefore, the ATP-promoted isomerization of the Mt·Eg5·ATP collision complex likely produces a series of structural changes in the Eg5 motor domain that favors movement of the neck linker.

The amplitude of the exponential phase of each pulse−chase transient provides quantitative information about the concentration of Eg5 sites that report during the first ATP turnover event. The maximum amplitude of the burst phase was 0.75 ADP/site (Figure 3B, inset), which was similar to the maximum amplitude of our acid−quench transients (Figure 4B, inset). The maximum burst amplitude observed in these experiments indicates that the entire Mt·Eg5 population bound MgATP tightly in these reactions (see Figure 4C and discussion of acid−quench burst amplitude below).

*ATP Hydrolysis Is a Relatively Fast Step in the Mt·Eg5-367 Mechanism.* We performed acid−quench experiments as a function of [α-$^{32}$P]MgATP concentration (Figure 4). The initial exponential burst of product formation correlates to the formation of [α-$^{32}$P]ADP·P$_i$ at the active site of Eg5 during the first ATP turnover. This exponential phase is followed by a slower linear phase, which corresponds to subsequent ATP turnovers. For conventional kinesin and Eg5, the microtubule-activated steady-state turnover is so fast that the pre-steady-state burst phase was obscured (*9*, *52*). Therefore, to visualize the initial burst phase, additional KCl was included in the ATP syringe to weaken motor rebinding to the microtubule after the first ATP turnover and, thereby, lowering the rate of the linear phase and steady-state turnover. We showed previously that the additional 100 mM salt does not alter the kinetics of ATP binding and ATP hydrolysis during the first ATP turnover (*9*, *56*). Figure 4B shows that the observed rate of ATP hydrolysis increased as a function of MgATP concentration with a maximum observed rate constant at 10.2 s$^{-1}$. The Figure 4B inset

Table 2: Intrinsic Rate Constants of the Mt·Eg5-367 ATPase Pathway

$$M\cdot E + ATP \overset{k_{+1}}{\rightleftharpoons} M\cdot E\cdot ATP \overset{k_{+1'}}{\rightleftharpoons} M\cdot E^{*}\cdot ATP \overset{k_{+2}}{\rightleftharpoons} M\cdot E\cdot ADP\cdot P_i \overset{k_{slow}}{\rightleftharpoons} M + E\cdot ADP + P_i$$

| | $k_+$ | $k_-$ |
|---|---|---|
| 1. ATP binding | $1\ \mu M^{-1}\ s^{-1}$ | |
| 1′. ATP-promoted isomerization | $18\ s^{-1}$ | |
| 2. ATP hydrolysis | $20-22\ s^{-1}$ | |
| 3. phosphate release coupled to dissociation | $6.5\ s^{-1}$ | |

illustrates that the burst amplitude also increased as a function of ATP concentration with the maximum burst amplitude at 0.75 per active site. We analyzed the ATP hydrolysis kinetics at three MgATP concentrations (Figure 4C) using the four-step model presented in eq 3 and Table 2. This analysis predicted an intrinsic rate constant for ATP hydrolysis, $k_{+2} = 20-22\ s^{-1}$, and the slow step that follows ATP hydrolysis at $6.5\ s^{-1}$. These constants provided $k_{cat} = 4.9-5\ s^{-1}$ based on eq 4, which was consistent with the experimentally determined $k_{cat}$ at $5.4\ s^{-1}$ (Figure 1, Table 1). The KINSIM analysis also predicted a reduced burst amplitude which was observed experimentally at $A_0 = 0.75$ ADP/Eg5 site (Figure 4B) and calculated on the basis of eq 5 using the KINSIM-derived rate constants ($A_0 = 0.6$ ADP/Eg5 site).

At first glance the intrinsic rate constant for ATP hydrolysis at $20-22\ s^{-1}$ appears high in comparison to the experimentally observed constant at $10.2 \pm 0.7\ s^{-1}$ (Figure 4B, Table 1). However, if two steps occur in sequence and their intrinsic rates are of similar magnitude, then the observed rate of the second reaction is approximately half the intrinsic rate constant (*52*, *57*). The ATP-promoted isomerization at $\sim 20\ s^{-1}$ followed by ATP hydrolysis at $20-22\ s^{-1}$ is consistent with an observed rate constant for ATP hydrolysis at $9-11\ s^{-1}$ as shown by the fit of the data to the four-step model (Figure 4C). In addition, our previous studies with a longer monomeric Eg5 protein (Eg5-437) exhibited similar ATP hydrolysis kinetics as observed here for apoEg5-367 (*9*).

The magnitude of the burst amplitude also increased as a function of MgATP concentration (Figure 4B, inset), with the maximum amplitude at 0.75 ADP/site, consistent with the maximum amplitude of the pulse−chase transients (Figure 3B, inset). The burst amplitude is derived from the rate constants that govern the step of ATP binding ($k_{+1}$ and $k_{+1'}$), ATP hydrolysis ($k_{+2}$ and $k_{-2}$), and the rate constant of the slow step in the pathway after ATP hydrolysis that limits subsequent ATP turnovers ($k_{slow}$). If $k_{+2} \gg k_{slow}$ and $k_{-2}$ is very slow ($\leq 0.001\ s^{-1}$), then the amplitude approaches 1 ADP/site. However, as $k_{slow}$ increases relative to $k_{+2}$, the amplitude decreases from unity. Analysis of the data based on the four-step model in eqs 3 and 5 predicts the decrease in the burst amplitude to ~0.75 per Eg5 active site because of $k_{slow}$. Therefore, the steady-state ATPase kinetics (Figure 1), the pre-steady-state kinetics of ATP binding (Figure 3), and the pre-steady-state kinetics of ATP hydrolysis (Figure 4) indicate that the entire Mt·Eg5 population reports during the first ATP turnover as well as subsequent turnovers.

*$P_i$ Product Release and Motor Detachment from the Microtubule Exhibit Slow Rate-Limiting Kinetics.* To measure directly the kinetics of $P_i$ product release from the Mt·Eg5 complex, we performed stopped-flow experiments using the MDCC-PBP assay (*51*). In this coupled assay, ATP binds the active site of Eg5 followed by ATP hydrolysis. When $P_i$ is released to the solution, MDCC-PBP binds the $P_i$ rapidly and tightly, resulting in a fluorescence enhancement (Figure 5A,B). Because microtubules activate $k_{slow}$ and therefore subsequent turnovers, these experiments must be performed at low microtubule concentration and with additional salt to observe the burst of phosphate release from the active site of Eg5 during the first ATP turnover. We performed a $P_i$ release experiment at 200 $\mu$M MgATP in the presence and absence of additional KCl (Figure 5A). The additional salt added to the ATP syringe weakens Eg5 rebinding to the microtubule, thereby slowing the microtubule reassociation rate and therefore subsequent ATP turnovers. This experimental strategy was also used for the acid−quench experiments (Figure 4). In the presence of the additional KCl, the phosphate release data were biphasic and exhibited the burst kinetics expected if $P_i$ release were faster than a subsequent step which limited steady-state turnover. In the absence of the additional salt, the kinetics of $P_i$ product release were also biphasic, but the exponential phase was much longer. Note that the exponential phase of the +KCl transient superimposes on the initial 150 ms of the no KCl transient. These results indicate that the additional salt does not affect the first ATP turnover but lowers the rate of the linear phase which corresponds to subsequent ATP turnovers (Figure 5E,F). To determine the burst amplitude of the pre-steady-state kinetics of $P_i$ release, the observed change in fluorescence intensity was converted to units of $P_i$ concentration using a $KH_2PO_4$ standard curve (data not shown). The burst amplitude of the exponential phase of the +KCl transient in Figure 5A was 0.68 $\mu$M $P_i$, which corresponds to ~1 $P_i$ per Eg5 site. In contrast, the amplitude of the transient in the absence of additional salt was 2.2 $\mu$M $P_i$ or ~4 $P_i$/Eg5 site, which is suggestive that the motor remained bound to the microtubule turning over multiple ATP molecules such that ~4 phosphates were released prior to Eg5 detachment from the microtubule. Additional evidence in support of this interpretation is that the $P_i$ burst rate in the presence of KCl was $7.1\ s^{-1}$, yet in the absence of additional salt it was significantly slower at $1.8\ s^{-1}$ because of the multiple turnovers. This kinetic profile was also observed for monomeric conventional Kinesin-1 (*4*). Moreover, the kinetics in Figure 5A provided confidence that this experimental strategy, i.e., including additional salt in the ATP syringe, could be used to measure the phosphate release kinetics for Eg5.

Figure 5B shows representative transients at varying ATP concentrations. Note that these transients show the lag for ATP binding and ATP hydrolysis and the burst of $P_i$ release during the first turnover, followed by a slower rate of $P_i$ release during subsequent turnovers. The observed burst rates of $P_i$ release during the first turnover increased as a function

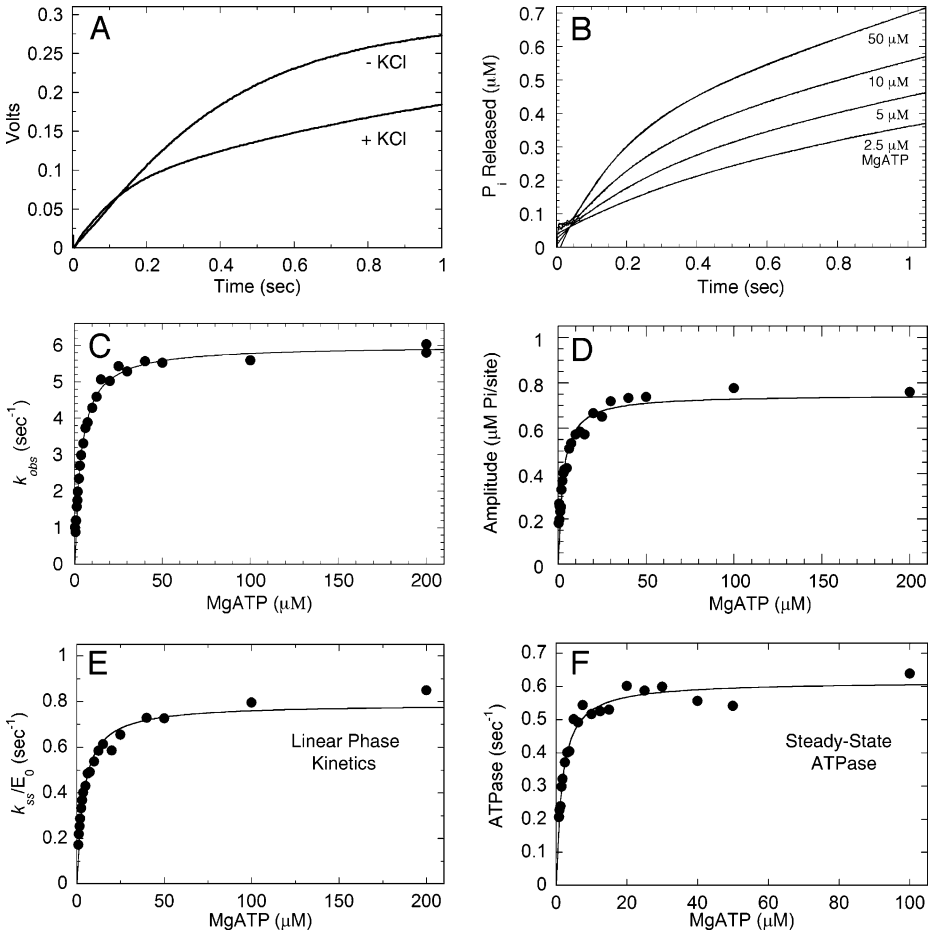


FIGURE 5: Kinetics of $P_i$ product release from the Mt·Eg5 complex. (A) A preformed Mt·Eg5 complex and MDCC-PBP were rapidly mixed with MgATP in the absence and presence of additional KCl, and the fluorescence enhancement of MDCC-PBP upon binding inorganic phosphate ($P_i$) was monitored in a stopped-flow instrument. Final concentrations: 0.5 $\mu$M apoEg5, 1 $\mu$M tubulin, 20 $\mu$M Taxol, 5 $\mu$M MDCC-PBP, 0.05 unit/mL PNPase, 250 $\mu$M MEG, 200 $\mu$M MgATP, and 0 or 100 mM KCl. In the presence of 100 mM KCl, the data displayed burst kinetics and were fit to eq 2, which provided $A_0 = 0.68$ $\mu$M $P_i$ (~1 $P_i$/Eg5 site), $k_b = 7.1 \pm 0.1$ $s^{-1}$, and $k_{ss}/E_0 = 0.63 \pm 0.01$ $s^{-1}$. In the absence of additional KCl, the data were fit to eq 2 with $k_{obs} = 1.8 \pm 0.01$ $s^{-1}$ and $A_0 = 2.2$ $\mu$M $P_i$ (~4/Eg5 site). (B) Shown are representative stopped-flow transients of $P_i$ product release from Mt·Eg5. MgATP concentrations are indicated. Final concentrations: 0.5 $\mu$M apoEg5, 1 $\mu$M tubulin, 20 $\mu$M Taxol, 5 $\mu$M MDCC-PBP, 0.05 unit/mL PNPase, 75 $\mu$M MEG, 0.3−200 $\mu$M MgATP, and 0 or 100 mM KCl. Each transient displayed burst kinetics and was fit to eq 2. (C) The observed exponential rate of $P_i$ product release was plotted versus MgATP concentration, and the data were fit to a hyperbolic function: $k_{b,max} = 6.0 \pm 0.1$ $s^{-1}$ and $K_{1/2,ATP} = 3.7 \pm 0.2$ $\mu$M. (D) The amplitude of the rapid exponential phase of each transient was plotted as a function of MgATP concentration: $A_{0,max} = 0.75 \pm 0.01$ $P_i$/Eg5 site. (E) The rate of the linear phase ($k_{ss}$) divided by the apoEg5 site concentration ($E_0$) was plotted against MgATP concentration: $k_{ss,max} = 0.79 \pm 0.02$ $s^{-1}$ and $K_{1/2,ATP} = 3.9 \pm 0.3$ $\mu$M. (F) Steady-state ATPase kinetics under similar reaction conditions of the $P_i$ release experiments. Final concentrations: 0.5 $\mu$M apoEg5, 1 $\mu$M tubulin, 20 $\mu$M Taxol, 0.05 unit/mL PNPase, 75 $\mu$M MEG, 0.8−100 $\mu$M [$\alpha$-$^{32}$P]MgATP, and 100 mM KCl. The data were fit to eq 1: $k_{cat} = 0.61 \pm 0.01$ $s^{-1}$ and $K_{1/2,ATP} = 1.1 \pm 0.1$ $\mu$M.

of MgATP concentration with $k_{obs,max} = 6.0$ $s^{-1}$ (Figure 4B,C). This rate constant is similar to steady-state turnover at 5.4 $s^{-1}$ (Figure 1). The burst amplitude of the exponential phase of $P_i$ release was converted from the observed change in fluorescence intensity (volts) to units of $P_i$ concentration using a $KH_2PO_4$ standard curve. The maximum amplitude of the exponential burst of $P_i$ product release during the first ATP turnover event was 0.75 $P_i$/site, consistent with the ATP binding and ATP hydrolysis kinetics reported in Figures 3 and 4, respectively, and Tables 1 and 2. These results indicate that this burst amplitude represents one ATP turnover by one apoEg5 active site. We have observed some variability in the maximum burst amplitude as seen by comparison of the +KCl transient in Figure 5A and those in Figure 5B,D. These experiments were done on different days. However, when experiments were done with a complete ATP concentration series on the same day, the maximum $P_i$ amplitude was consistently measured at ~0.75 $P_i$/Eg5 site.

The linear phase of the $P_i$ transients represents subsequent ATP turnovers. The rate of each transient was converted from volts·$s^{-1}$ to $\mu$M $P_i$·$s^{-1}$ and divided by the apoEg5 concentration used in the experiment (Figure 5E). The rate of the linear phase increased hyperbolically as a function of ATP concentration with the maximal $k_{ss}/E_0 = 0.79$ $s^{-1}$. This constant agreed well with the steady-state $k_{cat}$ at 0.61 $s^{-1}$ measured at the same experimental conditions with 100 mM KCl and the microtubule concentration at 1 $\mu$M tubulin polymer (Figure 5F). These results provide additional evidence that the experimental design to measure the phosphate release kinetics is valid, and it is the kinetics of the subsequent turnovers that are altered by the higher salt and lower microtubule concentrations rather than the first ATP turnover.

To measure the kinetics of the ATP-promoted dissociation of the Mt·Eg5 complex (Figure 6), additional salt was also included in the ATP syringe to weaken rebinding of the motor to the microtubule and, therefore, slow subsequent

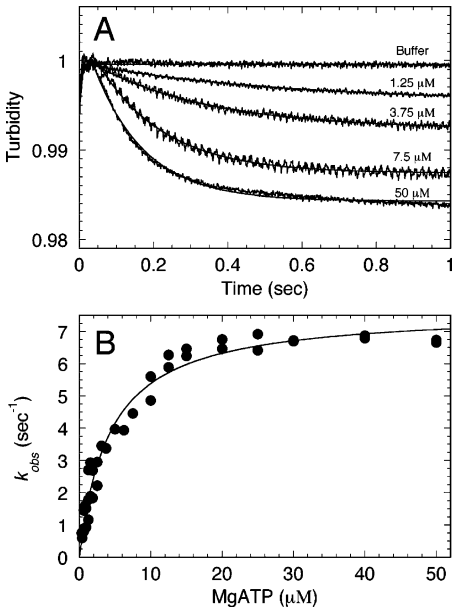


FIGURE 6: ATP-promoted dissociation of the Mt·Eg5-367 complex. (A) Preformed Mt·Eg5 complexes were rapidly mixed in a stopped-flow instrument with varying concentrations of MgATP plus KCl, and solution turbidity was monitored as a function of time. Final concentrations: 0.25 $\mu$M apoEg5, 0.25 $\mu$M tubulin for 0.3−1.3 $\mu$M MgATP, 0.5 $\mu$M apoEg5, 0.5 $\mu$M tubulin for 0.6−2.5 $\mu$M MgATP, 1 $\mu$M apoEg5, 1 $\mu$M tubulin for 1.6−10 $\mu$M MgATP, 2 $\mu$M apoEg5, 2 $\mu$M tubulin for 2.5−200 $\mu$M MgATP, 20 $\mu$M Taxol, and 100 mM KCl. Each transient was fit to a single-exponential function. (B) The rate of the rapid exponential phase of Mt·Eg5 dissociation was plotted as a function of MgATP concentration, and the data were fit to a hyperbola: $k_{obs,max} = 7.7 \pm 0.2$ s$^{-1}$ and $K_{1/2,ATP} = 4.2 \pm 0.3$ $\mu$M.

turnovers. The observed rate of motor detachment from the microtubule increased as a function of ATP concentration with the maximum rate at 7.7 s$^{-1}$. This observed maximum rate was similar to phosphate release at 6 s$^{-1}$ and the steady-state $k_{cat}$ at 5.4 s$^{-1}$ (Table 1).

## DISCUSSION

We have investigated the microtubule-activated behavior of human Eg5-367 that was purified in the nucleotide-free state (apoEg5) using a combination of steady-state and pre-steady-state kinetic methodologies. The results presented here indicate that the purified apoEg5 protein is fully active. We have defined the kinetics of apoEg5 association with microtubules, MgATP binding, ATP hydrolysis, $P_i$ product release, and ATP-promoted dissociation of the Mt·Eg5-367 complex (Scheme 1, Tables 1 and 2).

*ApoEg5 Protein Is Fully Active.* There are several lines of evidence presented in our previous study using apoEg5 in the absence of microtubules (*43*) and in this paper in the presence of microtubules that support the argument for apoEg5 protein being fully active. (1) Analytical gel filtration experiments to resolve the purified apoEg5 protein show no detectable peak at the elution volume corresponding to the void volume of the column (see Figure 1A from ref *43*). If apoEg5 were unfolding, we would expect to see aggregates of the degraded protein in the void volume. In contrast, these results indicate that the entire population of apoEg5 protein is soluble, homogeneous, and monodisperse. (2) ApoEg5 binds microtubules in a concentration-dependent manner (Figure 2). (3) The microtubule-activated steady-state ATPase of apoEg5 does not differ from previously characterized Eg5·ADP (Figure 1). (4) We observe full burst amplitudes in pulse−chase (Figure 3), acid−quench (Figure 4), and $P_i$ product release (Figure 5) experiments. (5) The apoEg5 motor domain has the ability to detach from the microtubule in an ATP concentration-dependent manner (Figure 6). Taken together, these results provide a powerful argument that the purification strategy to isolate nucleotide-free Eg5 has not altered the enzymatic capacity of the motor. In addition, these results suggest that, in spite of the amino acid sequence similarity of the catalytic core of kinesins, Eg5 is intrinsically more stable structurally when nucleotide is removed in comparison to either conventional Kinesin-1 or Kinesin-14 *Drosophila* Ncd.

*Microtubules Activate Each Step in the ATPase Pathway.* Typically, kinesin motors are purified in the absence of microtubules with ADP bound to the nucleotide binding site (*53*). Upon binding to the microtubule lattice, ADP is released rapidly from the active site to form the nucleotide-free state. For Eg5, microtubules significantly enhance the rate of ADP product release from 0.1 s$^{-1}$ (*43*) to 45 s$^{-1}$ (*9*). However, the behavior of apoEg5 off the microtubule is dramatically different when compared to microtubule-activated apoEg5. In the absence of microtubules, we observed approximately 15% of the apoEg5 enzyme sites binding and hydrolyzing ATP during the first turnover (*43*), whereas this same preparation in the presence of microtubules showed that 100% of motor population did bind and hydrolyze ATP (Figures 1 and 3−5). In fact, the results in Table 1 show that each step of the Eg5 ATPase cycle is accelerated dramatically by the Eg5−microtubule interaction rather than just a single step. These data clearly indicate that interaction with the microtubule alters the active site of Eg5 to promote and accelerate ATP turnover.

Rosenfeld et al. (*10*) proposed three distinct neck-linker conformations that are favored during the Eg5 ATPase cycle: (1) "perpendicular", an orientation perpendicular to the long axis of the motor domain based on the Turner et al. crystal structure (*58*); (2) "docked", where the neck linker docks onto the motor domain similar to Kif1a·AMPPNP (*59*) based on the Yan et al. and Cox et al. structures (*32*, *60*); and (3) "rigor", a conformation intermediate between perpendicular and docked that occurs when Eg5 is bound to the microtubule in a nucleotide-free state (*10*). Rosenfeld et al. (*10*) argued for a transition in the neck-linker orientation from perpendicular to rigor that occurred with microtubule binding. These results suggest that structural rearrangements in the Eg5 motor core that promote the rigor orientation of the neck linker are necessary to facilitate ATP binding. Therefore, the pathway of conformational communication in the Eg5 motor domain links the position of the neck linker to the three-dimensional structural arrangement of amino acids at the active site, thus providing a mechanism to couple the ATPase cycle with the structural transitions that drive movement. This linkage would be important to coordinate the action of each motor domain of dimeric Eg5 with the microtubule lattice. In addition, it would provide a sensitive means to communicate within the homotetramer through the coiled-coil from one dimeric unit on one microtubule to the other Eg5 dimer on the opposing microtubule.

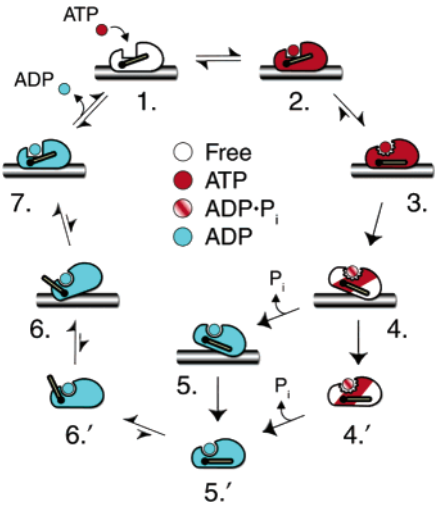


FIGURE 7: Model for the Mt·Eg5 ATPase cycle. ATP binding to the Mt·Eg5 complex occurs in at least two discrete steps: a weak collision event followed by ATP-promoted conformational change. ATP hydrolysis is a relatively fast step in the pathway. Following ATP hydrolysis, the coupled steps of $P_i$ product release and Eg5 detachment are shown in two possible sequential orders. Upon detachment from the microtubule, a rapid isomerization of the motor domain likely occurs to reach a competent state for rebinding the microtubule lattice. Microtubule binding occurs rapidly, followed by rapid ADP product release from the Eg5 active site to complete the cycle. The neck-linker conformations along the ATPase pathway are inferred from previous studies (*10*, *32*, *58*, *60*, *61*).

*The Rate-Limiting Step Corresponds to $P_i$ Release Coupled to Eg5 Detachment from the Microtubule.* Most steps in the ATPase cycle of monomeric Eg5 are relatively fast, including Eg5 association with the microtubule (Figure 2), ADP product release (*9*), MgATP binding (Figure 3), and ATP hydrolysis (Figure 4). The maximum observed rate of $P_i$ release ($k_{+3} = 6$ s$^{-1}$; Scheme 1, Figure 5) was similar to the maximum rate of steady-state ATP turnover ($k_{cat} = 5.4$ s$^{-1}$; Figure 1). The observed rate of ATP-promoted dissociation of the Mt·Eg5 complex was also similar in magnitude ($k_{+3} = 7.7$ s$^{-1}$; Figure 6B). The MgATP concentration dependence from these independent assays also provided similar apparent equilibrium constants: $K_{1/2,ATP} = 3.7$ $\mu$M for $P_i$ release experiments and 4.2 $\mu$M for ATP-promoted dissociation experiments. These results suggest that the two steps are coupled with a relatively slow rate-limiting step after ATP hydrolysis, followed by a fast step that must be >10-fold faster (Figure 7). Similar kinetics were initially observed for conventional Kinesin-1, K401, and the steps of $P_i$ release and motor detachment from the microtubule were also proposed to be coupled (*52*). However, an analysis of conventional K401 mutants that uncoupled motor detachment from phosphate release revealed that phosphate release was the rate-limiting step in the pathway (*50*). Phosphate release may be rate limiting for Eg5, and this hypothesis is consistent with the Mt·Eg5 cosedimentation studies using dimeric Eg5 where the ADP intermediate was more weakly bound to the microtubule (*44*). However, at this time we do not have the experimental evidence to order these steps for Eg5. Regardless, the slow step at 6−8 s$^{-1}$ in the mechanism, measured by both experiments, represents the rate-limiting step in the ATPase pathway (Tables 1 and 2, Figure 7).

We propose that after Eg5 releases $P_i$ from the active site and detaches from the microtubule as the Eg5·ADP intermediate, the motor domain undergoes a relatively rapid conformational change ($k_{+5'}$, Figure 7) to form a state that will rapidly and effectively rebind the microtubule lattice. The kinetics of this isomerization event were not determined in this study. However, Rosenfeld et al. (*10*) suggested that this step proceeds forward rapidly at 28−33 s$^{-1}$, which is consistent with our overall ATPase mechanism. Eg5 association with the microtubule (Figure 2) followed by rapid ADP product release complete the cycle (Figure 7).

The overall kinetic profile of monomeric Eg5 indicates that its interaction with the microtubule lattice accelerates the structural transitions required to meet the demand of ATP turnover during mitosis. In addition, the kinetics indicate that the motor spends a majority of its ATPase cycle bound to the microtubule, thus implicating the Eg5 homotetramer capable of processive movement between parallel or antiparallel microtubules. In fact, Valentine and Fordyce et al. recently reported that single molecules of dimeric Eg5 step processively along microtubules and remained processive even when subjected to strong loads (*45*). The results reported here suggest that the two motor domains of the Eg5 dimer would likely have one domain bound at any given time to support processive movement along the microtubule.

## ACKNOWLEDGMENT

We thank our colleagues Lisa R. Sproul and David Close for intellectual discussions and helpful comments during this study. We also acknowledge the anonymous reviewers whose critical comments significantly improved the manuscript.

## REFERENCES

1. Vale, R. D., and Fletterick, R. J. (1997) The design plan of kinesin motors, *Annu. Rev. Cell Dev. Biol. 13*, 745−777.
2. Vale, R. D., and Milligan, R. A. (2000) The way things move: Looking under the hood of molecular motor proteins, *Science 288*, 88−95.
3. Moyer, M. L., Gilbert, S. P., and Johnson, K. A. (1996) Purification and characterization of two monomeric kinesin constructs, *Biochemistry 35*, 6321−6329.
4. Moyer, M. L., Gilbert, S. P., and Johnson, K. A. (1998) Pathway of ATP hydrolysis by monomeric and dimeric kinesin, *Biochemistry 37*, 800−813.
5. Ma, Y.-Z., and Taylor, E. W. (1997) Kinetic mechanism of a monomeric kinesin construct, *J. Biol. Chem. 272*, 717−723.
6. Crevel, I. M., Nyitrai, M., Alonso, M. C., Weiss, S., Geeves, M. A., and Cross, R. A. (2004) What kinesin does at roadblocks: the coordination mechanism for molecular walking, *EMBO J. 23*, 23−32.
7. Jiang, W., and Hackney, D. D. (1997) Monomeric kinesin head domains hydrolyze multiple ATP molecules before release from a microtubule, *J. Biol. Chem. 272*, 5616−5621.
8. Rosenfeld, S. S., Jefferson, G. M., and King, P. H. (2001) ATP reorients the neck linker of kinesin in two sequential steps, *J. Biol. Chem. 276*, 40167−40174.
9. Cochran, J. C., Sontag, C. A., Maliga, Z., Kapoor, T. M., Correia, J. J., and Gilbert, S. P. (2004) Mechanistic analysis of the mitotic kinesin Eg5, *J. Biol. Chem. 279*, 38861−38870.
10. Rosenfeld, S. S., Xing, J., Jefferson, G. M., and King, P. H. (2005) Docking and rolling, a model of how the mitotic motor Eg5 works, *J. Biol. Chem. 280*, 35684−35695.
11. Stock, M. F., Chu, J., and Hackney, D. D. (2003) The kinesin family member BimC contains a second microtubule binding region attached to the N terminus of the motor domain, *J. Biol. Chem. 278*, 52315−52322.
12. Pechatnikova, E., and Taylor, E. W. (1997) Kinetic mechanism of monomeric non-claret disjunctional protein (Ncd) ATPase, *J. Biol. Chem. 272*, 30735−30740.

13. Mackey, A. T., and Gilbert, S. P. (2000) Moving may require two heads: A kinetic investigation of monomeric Ncd, *Biochemistry 39*, 1346−1355.
14. Mackey, A. T., and Gilbert, S. P. (2003) The ATPase crossbridge cycle of the Kar3 motor domain: implications for single-headed motility, *J. Biol. Chem. 278*, 3527−3535.
15. Mackey, A. T., Sproul, L., Sontag, C., Satterwhite, L., Correia, J. J., and Gilbert, S. P. (2004) Mechanistic analysis of the *Saccharomyces cerevisiae* kinesin Kar3, *J. Biol. Chem. 279*, 51354−51361.
16. Cole, D. G., Saxton, W. M., Sheehan, K. B., and Scholey, J. M. (1994) A "slow" homotetrameric kinesin-related motor protein purified from *Drosophila* embryos, *J. Biol. Chem. 269*, 22913−22916.
17. Kashina, A., Baskin, R. J., Cole, D., Wedaman, K., Saxton, W., and Scholey, J. (1996) A bipolar kinesin, *Nature 379*, 270−272.
18. Gordon, D. M., and Roof, D. M. (1999) The kinesin-related protein Kip1p of *Saccharomyces cerevisiae* is bipolar, *J. Biol. Chem. 274*, 28779−28786.
19. Blangy, A., Lane, H. A., d'Herin, P., Harper, M., Kress, M., and Nigg, E. A. (1995) Phosphorylation by $p34^{cdc2}$ regulates spindle association of human Eg5, a kinesin-related motor essential for bipolar spindle formation in vivo, *Cell 83*, 1159−1169.
20. Sawin, K. E., LeGuellec, K., Philippe, M., and Mitchison, T. J. (1992) Mitotic spindle organization by a plus-end-directed microtubule motor, *Nature 359*, 540−543.
21. Saunders, W. S., and Hoyt, M. A. (1992) Kinesin-related proteins required for structural integrity of the mitotic spindle, *Cell 70*, 451−458.
22. Mountain, V., Simerly, C., Howard, L., Ando, A., Schatten, G., and Compton, D. A. (1999) The Kinesin-related protein, HSET, opposes the activity of Eg5 and cross-links microtubules in the mammalian mitotic spindle, *J. Cell Biol. 147*, 351−365.
23. Sharp, D. J., McDonald, K. L., Brown, H. M., Matthies, H. J., Walczak, C., Vale, R., Mitchison, T. J., and Scholey, J. M. (1999) The bipolar kinesin, KLP61F, cross-links microtubules within interpolar microtubule bundles of *Drosophila* embryonic mitotic spindles, *J. Cell Biol. 144*, 125−138.
24. Sharp, D. J., Yu, K. R., Sisson, J. C., Sullivan, W., and Scholey, J. M. (1999) Antagonistic microtubule-sliding motors position mitotic centrosomes in *Drosophila* early embryos, *Nat. Cell Biol. 1*, 51−54.
25. Kapitein, L. C., Peterman, E. J., Kwok, B. H., Kim, J. H., Kapoor, T. M., and Schmidt, C. F. (2005) The bipolar mitotic kinesin Eg5 moves on both microtubules that it crosslinks, *Nature 435*, 114−118.
26. Kwok, B. H., Yang, J. G., and Kapoor, T. M. (2004) The rate of bipolar spindle assembly depends on the microtubule-gliding velocity of the mitotic kinesin Eg5, *Curr. Biol. 14*, 1783−1788.
27. Miyamoto, D. T., Perlman, Z. E., Burbank, K. S., Groen, A. C., and Mitchison, T. J. (2004) The kinesin Eg5 drives poleward microtubule flux in *Xenopus laevis* egg extract spindles, *J. Cell Biol. 167*, 813−818.
28. Chakravarty, A., Howard, L., and Compton, D. A. (2004) A mechanistic model for the organization of microtubule asters by motor and non-motor proteins in a mammalian mitotic extract, *Mol. Biol. Cell 15*, 2116−2132.
29. Crevel, I. M. T. C., Lockhart, A., and Cross, R. A. (1997) Kinetic evidence for low chemical processivity in ncd and Eg5, *J. Mol. Biol. 273*, 160−170.
30. Lockhart, A., and Cross, R. A. (1996) Kinetics and mMotility of the Eg5 microtubule motor, *Biochemistry 35*, 2365−2373.
31. Cox, C. D., Torrent, M., Breslin, M. J., Mariano, B. J., Whitman, D. B., Coleman, P. J., Buser, C. A., Walsh, E. S., Hamilton, K., Schaber, M. D., Lobell, R. B., Tao, W., South, V. J., Kohl, N. E., Yan, Y., Kuo, L. C., Prueksaritanont, T., Slaughter, D. E., Li, C., Mahan, E., Lu, B., and Hartman, G. D. (2006) Kinesin spindle protein (KSP) inhibitors. Part 4: Structure-based design of 5-alkylamino-3,5-diaryl-4,5-dihydropyrazoles as potent, water-soluble inhibitors of the mitotic kinesin KSP, *Bioorg. Med. Chem. Lett. 16*, 3175−3179.
32. Cox, C. D., Breslin, M. J., Mariano, B. J., Coleman, P. J., Buser, C. A., Walsh, E. S., Hamilton, K., Huber, H. E., Kohl, N. E., Torrent, M., Yan, Y., Kuo, L. C., and Hartman, G. D. (2005) Kinesin spindle protein (KSP) inhibitors. Part 1: The discovery of 3,5-diaryl-4,5-dihydropyrazoles as potent and selective inhibitors of the mitotic kinesin KSP, *Bioorg. Med. Chem. Lett. 15*, 2041−2045.
33. Fraley, M. E., Garbaccio, R. M., Arrington, K. L., Hoffman, W. F., Tasber, E. S., Coleman, P. J., Buser, C. A., Walsh, E. S., Hamilton, K., Fernandes, C., Schaber, M. D., Lobell, R. B., Tao, W., South, V. J., Yan, Y., Kuo, L. C., Prueksaritanont, T., Shu, C., Torrent, M., Heimbrook, D. C., Kohl, N. E., Huber, H. E., and Hartman, G. D. (2006) Kinesin spindle protein (KSP) inhibitors. Part 2: the design, synthesis, and characterization of 2,4-diaryl-2,5-dihydropyrrole inhibitors of the mitotic kinesin KSP, *Bioorg. Med. Chem. Lett. 16*, 1775−1779.
34. Garbaccio, R. M., Fraley, M. E., Tasber, E. S., Olson, C. M., Hoffman, W. F., Arrington, K. L., Torrent, M., Buser, C. A., Walsh, E. S., Hamilton, K., Schaber, M. D., Fernandes, C., Lobell, R. B., Tao, W., South, V. J., Yan, Y., Kuo, L. C., Prueksaritanont, T., Slaughter, D. E., Shu, C., Heimbrook, D. C., Kohl, N. E., Huber, H. E., and Hartman, G. D. (2006) Kinesin spindle protein (KSP) inhibitors. Part 3: synthesis and evaluation of phenolic 2,4-diaryl-2,5-dihydropyrroles with reduced hERG binding and employment of a phosphate prodrug strategy for aqueous solubility, *Bioorg. Med. Chem. Lett. 16*, 1780−1783.
35. Mayer, T. U., Kapoor, T. M., Haggarty, S. J., King, R. W., Schreiber, S. L., and Mitchison, T. J. (1999) Small molecule inhibitor of mitotic spindle bipolarity identified in a phenotype-based screen, *Science 286*, 971−974.
36. Sakowicz, R., Finer, J. T., Beraud, C., Crompton, A., Lewis, E., Fritsch, A., Lee, Y., Mak, J., Moody, R., Turincio, R., Chabala, J. C., Gonzales, P., Roth, S., Weitman, S., and Wood, K. W. (2004) Antitumor activity of a kinesin inhibitor, *Cancer Res. 64*, 3276−3280.
37. Nakazawa, J., Yajima, J., Usui, T., Ueki, M., Takatsuki, A., Imoto, M., Toyoshima, Y. Y., and Osada, H. (2003) A novel action of terpendole E on the motor activity of mitotic kinesin Eg5, *Chem. Biol. 10*, 131−137.
38. Gartner, M., Sunder-Plassmann, N., Seiler, J., Utz, M., Vernos, I., Surrey, T., and Giannis, A. (2005) Development and biological evaluation of potent and specific inhibitors of mitotic Kinesin Eg5, *ChemBioChem. 6*, 1173−1177.
39. Sunder-Plassmann, N., Sarli, V., Gartner, M., Utz, M., Seiler, J., Huemmer, S., Mayer, T. U., Surrey, T., and Giannis, A. (2005) Synthesis and biological evaluation of new tetrahydro-beta-carbolines as inhibitors of the mitotic kinesin Eg5, *Bioorg. Med. Chem. 13*, 6094−6111.
40. Skoufias, D. A., DeBonis, S., Saoudi, Y., Lebeau, L., Crevel, I., Cross, R., Wade, R. H., Hackney, D., and Kozielski, F. (2006) *S*-Trityl-L-cysteine is a reversible, tight-binding inhibitor of the human kinesin Eg5 that specifically blocks mitotic progression, *J. Biol. Chem. 281*, 17559−17569.
41. Duhl, D. M., and Renhowe, P. A. (2005) Inhibitors of kinesin motor proteins−research and clinical progress, *Curr. Opin. Drug Discov. Dev. 8*, 431−436.
42. Bergnes, G., Brejc, K., and Belmont, L. (2005) Mitotic kinesins: prospects for antimitotic drug discovery, *Curr. Top. Med. Chem. 5*, 127−145.
43. Cochran, J. C., and Gilbert, S. P. (2005) ATPase mechanism of Eg5 in the absence of microtubules: insight into microtubule activation and allosteric inhibition by monastrol, *Biochemistry 44*, 16633−16648.
44. Krzysiak, T. C., Wendt, T., Sproul, L. R., Tittmann, P., Gross, H., Gilbert, S. P., and Hoenger, A. (2006) A structural model for monastrol inhibition of dimeric kinesin Eg5, *EMBO J. 25*, 2263−2273.
45. Valentine, M. T., Fordyce, P. M., Krzysiak, T. C., Gilbert, S. P., and Block, S. M. (2006) Individual dimers of the mitotic kinesin motor Eg5 step processively and support substantial loads in vitro, *Nat. Cell Biol. 8*, 470−476.
46. Maliga, Z., Kapoor, T. M., and Mitchison, T. J. (2002) Evidence that monastrol is an allosteric inhibitor of the mitotic kinesin Eg5, *Chem. Biol. 9*, 989−996.
47. Gilbert, S. P., and Mackey, A. T. (2000) Kinetics: a tool to study molecular motors, *Methods 22*, 337−354.
48. Foster, K. A., Correia, J. J., and Gilbert, S. P. (1998) Equilibrium binding studies of non-claret disjunctional protein (Ncd) reveal cooperative interactions between the motor domains, *J. Biol. Chem. 273*, 35307−35318.
49. Barshop, B. A., Wrenn, R. F., and Frieden, C. (1983) Analysis of numerical methods for computer simulation of kinetic processes: Development of KINSIM−a flexible, portable system, *Anal. Biochem. 130*, 134−145.
50. Klumpp, L. M., Hoenger, A., and Gilbert, S. P. (2004) Kinesin's second step, *Proc. Natl. Acad. Sci. U.S.A. 101*, 3444−3449.

51. Brune, M., Hunter, J. L., Corrie, J. E. T., and Webb, M. R. (1994) Direct, real-time measurement of rapid inorganic phosphate release using a novel fluorescent probe and its application to actomyosin subfragment 1 ATPase, *Biochemistry 33*, 8262−8271.
52. Gilbert, S. P., Webb, M. R., Brune, M., and Johnson, K. A. (1995) Pathway of processive ATP hydrolysis by kinesin, *Nature 373*, 671−676.
53. Hackney, D. D. (1988) Kinesin ATPase: Rate-limiting ADP release, *Proc. Natl. Acad. Sci. U.S.A. 85*, 6314−6318.
54. Hackney, D. D., Malik, A.-S., and Wright, K. W. (1989) Nucleotide-free kinesin hydrolyzes ATP with burst kinetics, *J. Biol. Chem. 264*, 15943−15948.
55. Sadhu, A., and Taylor, E. W. (1992) A kinetic study of the kinesin ATPase, *J. Biol. Chem. 267*, 11352−11359.
56. Cochran, J., Gatial, J. I., Kapoor, T., and Gilbert, S. (2005) Monastrol inhibition of mitotic kinesin Eg5, *J. Biol. Chem. 280*, 12658−12667.
57. Johnson, K. A. (1992) Transient-state kinetic analysis of enzyme reaction pathways, *Enzymes 20*, 1−61.
58. Turner, J., Anderson, R., Guo, J., Beraud, C., Fletterick, R., and Sakowicz, R. (2001) Crystal structure of the mitotic spindle kinesin Eg5 reveals a novel conformation of the neck-linker, *J. Biol. Chem. 276*, 25496−25502.
59. Kikkawa, M., Sablin, E. P., Okada, Y., Yajima, H., Fletterick, R. J., and Hirokawa, N. (2001) Switch-based mechanism of kinesin motors, *Nature 411*, 439−445.
60. Yan, Y., Sardana, V., Xu, B., Homnick, C., Halczenko, W., Buser, C. A., Schaber, M., Hartman, G. D., Huber, H. E., and Kuo, L. C. (2004) Inhibition of a mitotic motor protein: where, how, and conformational consequences, *J. Mol. Biol. 335*, 547−554.
61. Maliga, Z., Xing, J., Cheung, H., Juszczak, L. J., Friedman, J. M., and Rosenfeld, S. S. (2006) A pathway of structural changes produced by monastrol binding to Eg5, *J. Biol. Chem. 281*, 7977−7982.

BI0608562